Available online at www.sciencedirect.com

ScienceDirect

Procedia Engineering 166 (2016) 83 – 90

Procedia Engineering

www.elsevier.com/locate/procedia

2nd International Symposium on Submerged Floating Tunnels and Underwater Tunnel Structures

Experiments and modeling on the maximum displacement of a long tensioned mooring tether subjected to vortex-induced vibration

Ling Kang[a,b], Fei Ge[a,*], Xiaodong Wu[c], Youshi Hong[a,b,†]

[a]*LNM, Institute of Mechanics, Chinese Academy of Sciences, Beijing 100190, China*
[b]*University of Chinese Academy of Sciences, Beijing, China,* [C]*Taiyuan University of Technology, Taiyuan 030024, China*

Abstract

The maximum root mean square (RMS) of the displacement of a long tensioned mooring tether undergoing vortex-induced vibration (VIV) as the flow velocity varies was experimentally investigated, and an evaluation model was established to predict the maximum RMS value of the displacement by a dimensionless analysis. The results showed that the maximum RMS of the displacement linearly increased with the increasing of the flow velocity if only the low order modes were excited at the corresponding flow velocities. This kind of maximum RMS of displacement was evaluated by the proposed model, which is more reliable when it was used to predict the maximum RMS of the total displacement.

Peer-review under responsibility of the organizing committee of SUFTUS-2016

Keywords: Long tensioned tether; vortex-induced vibration; displacement fluctuation; vibration mode; maximum displacement model

1. Introduction

Long tensioned mooring tethers are important components of engineering structures in deep oceans, such as deep sea platforms and submerged floating tunnels (SFT) [1], since they are designed to restrain the displacement and internal forces of the main bodies of deep ocean structures. Their safety has a close relation to the safety of the main bodies. One of the events that influence the safety of long tensioned mooring tethers is the vortex shedding of ocean currents passing through, which makes the tethers undergo vortex-induced vibration (VIV). Dynamic responses of the

* Corresponding author. Tel.: +86-10-82543968; fax: +86-10-62561284.
E-mail address: gefei@imech.ac.cn
* Corresponding author. Tel.: +86-10-82543966; fax: +86-10-62561284.
E-mail address: hongys@imech.ac.cn

Peer-review under responsibility of the organizing committee of SUFTUS-2016
doi:10.1016/j.proeng.2016.11.568

long tensioned tether subjected to VIV in recent investigations are stresses (strains) [2,3] and displacements induced in the process. For dynamic displacements, the focus was on the maximum root mean square (RMS) values, frequencies, dominant vibrations modes and wave types [4,5,6,7]. Wu et al.[8] summarized that the dynamic displacements of a long tensioned tether undergoing VIV were mainly characterized by multiple and high order modes, high harmonics and travelling waves in addition to standing waves. Dual resonance and non-resonance were studied as well [9]. However, the maximum RMS of the dynamic displacement of such tethers is not in-depth investigated.

In uniform flows, one concerned issue in VIV for a long tensioned tether with cylindrical shape is the effect of flow velocity on the maximum RMS of the displacement. Research results [6,9,10,11] showed that, as the uniform flow velocity increases, the maximum RMS of the displacement in both CF and IL directions increases in a saw tooth or fluctuating pattern. Such maximum value could be obtained by numerically solving the governing equations of the tether and the fluid field with the consideration of fluid-structure interaction [12,13]. However, it is a complicated and time-consuming work for the governing equations to be numerically solved. Therefore, a simpler and more direct evaluation model for the maximum RMS of the displacement of a long tensioned tether undergoing VIV is expected. In this paper, the maximum RMS of the displacement with the uniform flow velocity was first studied by an experiment. Then, according to the experimental results, a simple evaluation model was established to calculate the maximum RMS of the displacement of a long tensioned mooring tether undergoing VIV.

2. Experimental study

2.1. Experimental set-up and data Analysis

The experiment was carried out in a towing flume with the length of 29.0 m, the width of 4.5 m and the depth of 4.0 m [Fig. 1. (a)]. As shown in Fig. 1. (b), the test model was mounted on a towing car by universal joints. The state of uniform flows was attained by the towing car moving forward or backward along the length direction of the flume at a controllable constant speed. One end of the test model was connected with a cable and through pulleys the cable was hung with a steel weight inside a weight sleeve. By this set-up, the test model was tensioned.

An aluminum pipe with circular cross section was adopted as the experimental model, for which the length is 3.31 m, the outer diameter is 6 mm and the inner diameter is 4 mm. The axial tension had the value of 10 N. The uniform flow velocity varied from 0.1 m/s to 1.5 m/s with an increment of 0.1 m/s and numbered as 1 to 15 from 0.1 m/s successively. Table 1 summarizes the main parameters of the test model.

Fiber brag grating (FBG) strain sensors were stuck to the surface of the test model to measure the strains on the surface of the model. As illustrated in Fig. 1. (b), (c) and (d), 20 FBG sensors were installed at the CF direction and another 20 were at the IL direction with the sensor spacing of 160 mm. This arrangement implies that the test model is simplified as a 20-DOF damping system in each direction.

Table 1. Main parameters of test model

Experiment parameters	Symbol	Unit	Value
Length	l	m	3.31
Outer diameter	d_1	mm	6.0
Inner diameter	d_2	mm	4.0
Modulus of elasticity	E	GPa	71.0
Aspect ratio	l / d_1	-	551
Mass Ratio	m^*	-	1.5
Reynolds number	Re	-	600-9000

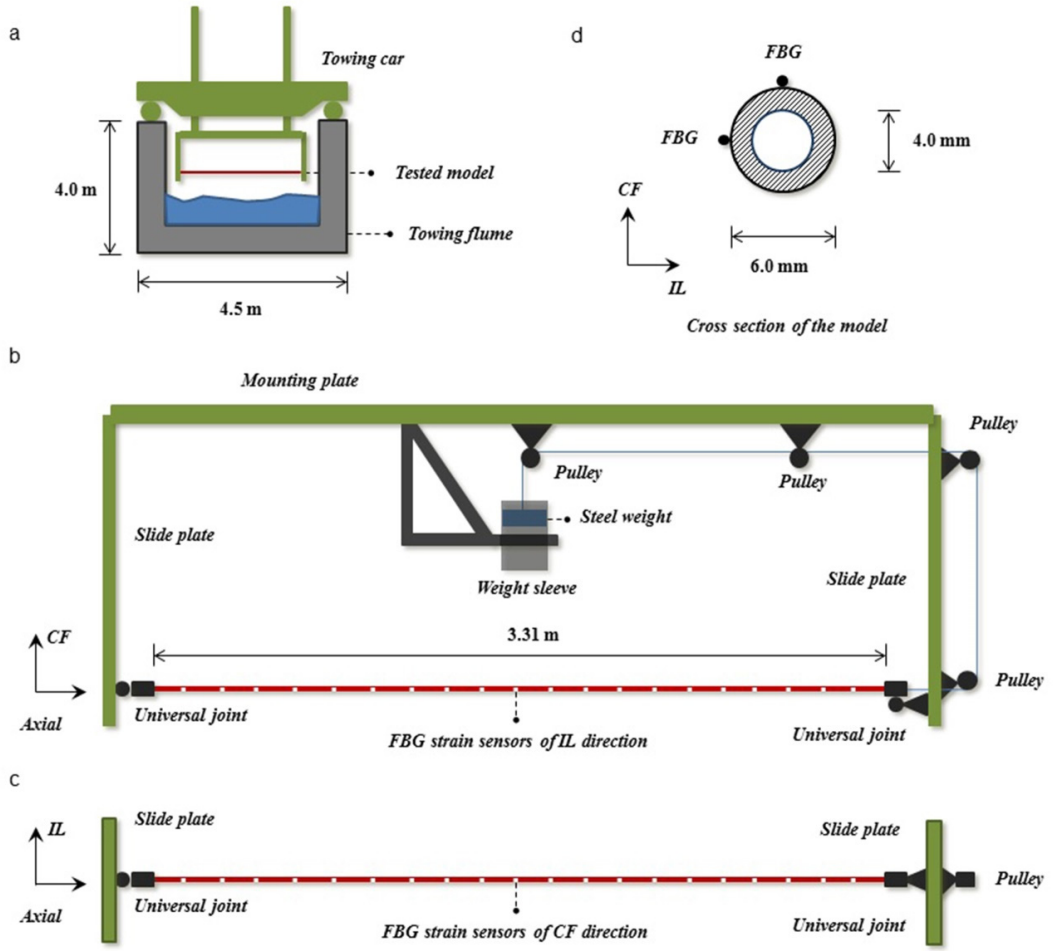

Fig. 1. Schematic of experimental set-up: (a) Towing flume with tested model being mounted on a towing car; (b) Front view of experimental set-up and arrangement of fiber brag grating (FBG) strain sensors of in-line (IL) direction along axial direction of test model; (c) Top view of experimental set-up and arrangement of FBG strain sensors of cross-flow (CF) direction along axial direction of test model; (d) Cross section of test model and arrangement of FBG strain sensors on cross section of test model.

The modal weight and displacement signals in CF and IL directions were extracted from the measured strain signals in the corresponding directions by the method employed in [6,14]. Moreover, the time series of the total displacement was calculated by Eq. (1):

$$u_{\mathrm{TOTAL},i}(k)=\sqrt{u_{\mathrm{CF},i}^2(k)+u_{\mathrm{IL},i}^2(k)},\quad k=1,2,\ldots,s,\quad i=1,2,\ldots,20 \tag{1}$$

where $u_{\mathrm{TOTAL},i}(k)$ is the total displacement, $u_{\mathrm{CF},i}(k)$ the displacement in CF direction and $u_{\mathrm{IL},i}(k)$ the displacement in IL direction at the discrete time k and the i-th sensor location. s is the total number of sample data.

The relative ratio of the amplitude of the n-th modal weight at a tested flow velocity was defined as the amplitude of the n-th modal weight at a tested flow velocity to the maximum amplitude within the amplitudes of all modal weights at the same flow velocity. The relative ratio of the amplitude was employed to identify the excited modes of the test model at a tested flow velocity.

2.2. Results

Fig. 2 (a) and (b) shows the maximum RMS of the displacement versus the flow velocity in CF direction and IL direction, respectively. The maximum RMS of the displacement was normalized by the outer diameter of the experimental model. In a general point of view, the maximum RMS values of the displacement in CF and IL directions increase with the increasing of flow velocity in a fluctuating pattern. This trend is in accordance with the result mentioned in Section 1. Fig. 2 (c) and (d) presents the relative ratio of the amplitude of the first eight modal weights versus the flow velocity and mode order in CF direction and IL direction, respectively. From these figures, the excited modes in CF and IL directions were found. In this paper, the excited mode is defined as the mode whose relative ratio of the amplitude is between the value of 0.1 and 1.0.

Comparing Fig. 2 (a) and (c) in CF direction and Fig. 2 (b) and (d) in IL direction, we found that within the flow velocity range (e.g. 0.6 – 0.9 m/s) where the fourth and upper modes are excited, the maximum RMS values of the displacement in CF and IL directions constitute the concave section of the curve. Moreover, if we use the maximum RMS values of the displacement in CF and IL directions at the flow velocities of 0.2 m/s to 0.5 m/s and 1.0 m/s, where only the modes with the order lower than the fourth are excited, to carry out a curve fitting, we find that those maximum RMS values of the displacement are linearly related to the flow velocity. They linearly increase as the flow velocity increases, as shown in Fig. 3 (a) and (b). So are the corresponding maximum RMS values of the total displacement [Fig. 3 (c)].

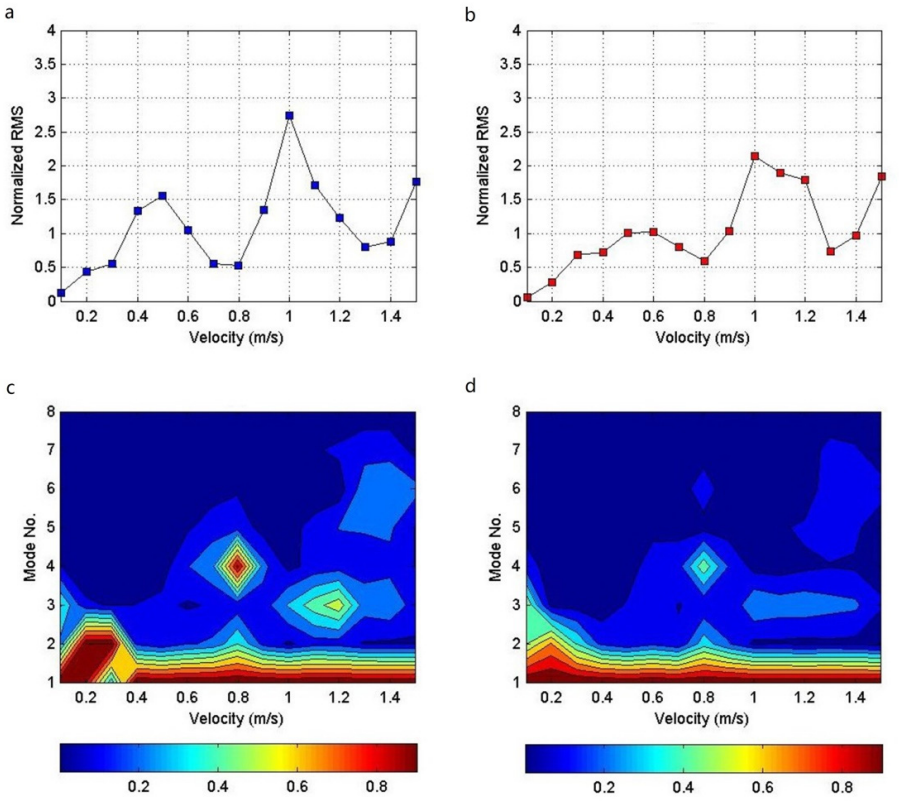

Fig. 2. (a) The maximum RMS of the displacement normalized by outer diameter of test model versus flow velocity in CF direction; (b) The maximum RMS of the displacement normalized by outer diameter of test model versus flow velocity in IL direction; (c) Relative ratios of the amplitude of the first eight modal weights versus flow velocity and mode number in CF direction; (d) Relative ratio of the amplitude of the first eight modal weights versus flow velocity and mode number in IL direction.

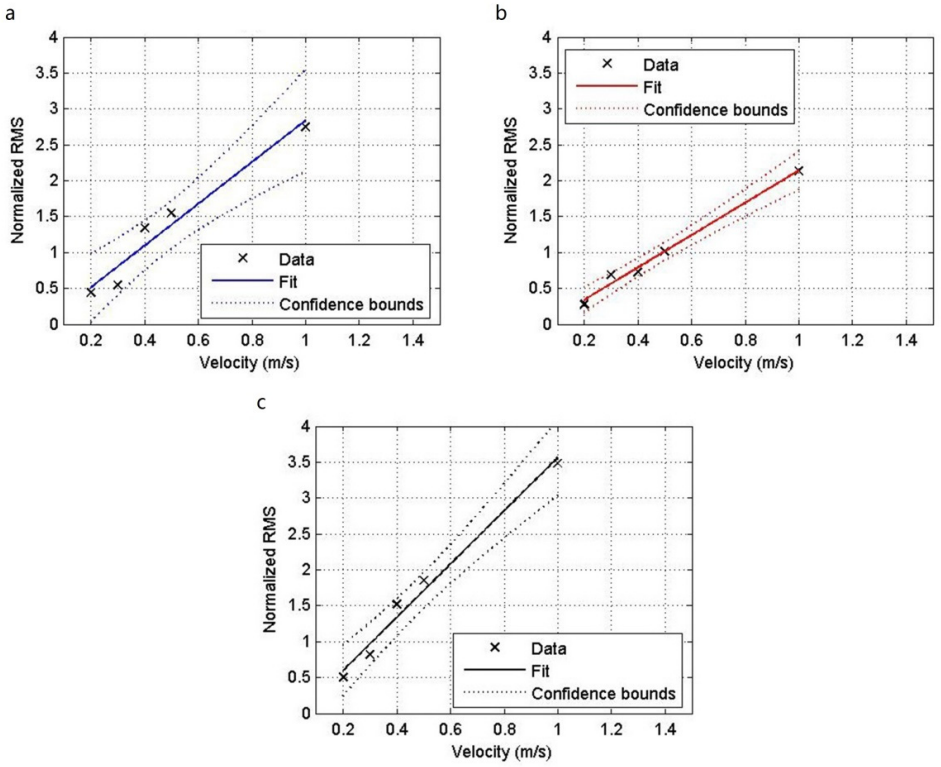

Fig. 3. Linear fit of the maximum RMSs of the displacement with respect to flow velocities where only modes with order lower than the fourth are excited: (a) in CF direction; (b) in IL direction; (c) of total displacement.

3. Modeling

3.1. Evaluation model

The dimensionless value $u_{\max}/d_1$ of the maximum RMS for the displacement in total or component directions is universally expressed as the following function.

$$\frac{u_{\max}}{d_1} = f\left(\frac{l}{d_1}, m^*, \zeta, \frac{Tl^2}{EI}, Re\right) \tag{2}$$

where ζ is the damping ratio and Tl^2/EI is a dimensionless parameter that indicates the type of the tether (string-like or beam-like) [15] with EI being the bending stiffness of the mooring tether.

Since the experimental result shows that the maximum RMS of the displacement linearly depends on the flow velocity where only the low order modes are excited, Reynolds number *Re*, which represents the flow velocity for a given dynamic system and fluid field, was taken out from the brackets of Eq.(2). Then, the conditioned maximum RMS of the displacement $u_{\max,c}$ is expressed as:

$$\frac{u_{\max,c}}{d_1} = \overline{f}\left(\frac{l}{d_1}, m^*, \zeta, \frac{Tl^2}{EI}\right) Re \tag{3}$$

The derived Eq. (4) shows the maximum displacement of a simple supported tensioned beam subjected to the static uniform force perpendicular to the spanwise direction of the beam.

$$u_{\max}^{\text{static}} = \alpha \frac{ql^2}{T} + \beta \frac{qEI}{T^2} = \left(\alpha \frac{l^2}{T} + \beta \frac{EI}{T^2} \right) q \tag{4}$$

where $u(x)$ is the static displacement along the spanwise axis of x. $u_{\max}^{\text{static}}$ is the static maximum displacement, q the static uniform force and α, β two constant coefficients.

Eq. (4) indicates that the static maximum displacement is linearly dependent on the static uniform force. Their slope is the linear combination of l^2/T and EI/T^2. Analogously, we assumed that the slope of Eq. (3) also has such linear combination form. Then, the terms ql^2/T and qEI/T^2 of Eq. (4) were transformed into Eqs. (5) and (6) by the dimensional homogeneity theory, respectively.

$$\frac{ql^2}{T} \sim \frac{\rho d_1^2 U f_{1\text{NF}} l^2}{T} = \frac{\rho d_1 U}{\mu} \frac{\mu f_{1\text{NF}}}{T/l^2} d_1 = Re \frac{\mu f_{1\text{NF}}}{T/l^2} d_1 \tag{5}$$

$$\frac{qEI}{T^2} \sim \frac{\rho d_1^2 U f_{1NF} EI}{T^2} = \frac{\rho d_1 U}{\mu} \frac{\mu f_{1\text{NF}} EI\left(l^4 EI\right)}{T^2\left(l^4 EI\right)} d_1 = Re \frac{\mu f_{1\text{NF}}}{EI/l^4} \frac{1}{\left(Tl^2/EI\right)^2} d_1 \sim Re \frac{\mu f_{1\text{NF}}}{E} \left(\frac{l}{d_1} \right)^4 \frac{1}{\left(Tl^2/EI\right)^2} d_1 \tag{6}$$

where μ is the dynamic viscosity coefficient of the fluid. $f_{1\text{NF}}$ represents the first natural frequency of the long tensioned tether. From Eqs. (3), (5) and (6) and the linear combination assumption, the slope $\bar{f}$ is written in the following form:

$$\bar{f} = c_1(\zeta) \frac{\mu f_{1\text{NF}}}{T/l^2} + c_2(\zeta) \frac{\mu f_{1\text{NF}}}{E} \left(\frac{l}{d_1} \right)^4 \left(\frac{Tl^2}{EI} \right)^{-2} = c_1(\zeta) p_1 + c_2(\zeta) p_2 \tag{7}$$

where c_1 and c_2 are two constant coefficients supposed to have the values determined by the damping ratio. The influence of the mass ratio has already been considered in the first natural frequency. Substituting Eq. (7) into Eq. (3), we obtain the evaluation model of the conditioned maximum RMS of the displacement in a dimensionless form, which is presented by Eq. (8).

$$\frac{u_{\max,c}}{d_1} = \left[c_1(\zeta) \frac{\mu f_{1\text{NF}}}{T/l^2} + c_2(\zeta) \frac{\mu f_{1\text{NF}}}{E} \left(\frac{l}{d_1} \right)^4 \left(\frac{Tl^2}{EI} \right)^{-2} \right] Re \tag{8}$$

The values of c_1 and c_2 can be determined by an experiment, though their relationships with respect to the damping ratio are unclear.

3.2. Values of c_1 and c_2

Eq. (7) indicates that, if two different fitting slops and the corresponding pairs of (p_1, p_2) are given, c_1 and c_2 are the solutions of the following system of linear equations.

$$\begin{pmatrix} p_{11} & p_{21} \\ p_{12} & p_{22} \end{pmatrix} \begin{pmatrix} c_1 \\ c_2 \end{pmatrix} = \begin{pmatrix} \bar{f}_1 \\ \bar{f}_2 \end{pmatrix} \tag{9}$$

Therefore, another two tests with tensions of 50 N and 75 N were conducted. The fitting slops for the cases with the tensions of 10 N and 50 N were used to evaluate c_1 and c_2. Results are listed in Table 2.

Table 2. Values of c_1 and c_2

Directions	Fitting slop ($\times 10^{-4}$)		Values	
	10 N	50 N	c_1	c_2 ($\times 10^{2}$)
CF	4.846	4.028	0.501	-2.202
IL	3.754	1.916	0.222	-0.434
TOTAL	6.176	5.511	0.690	-3.205

3.3. Model verification

The experimental values of the conditioned maximum RMS of the displacement in the case with the tension of 75 N were employed to verify those predicted by Eq. (8). Values of c_1 and c_2 in Table 2 were used. Note that the dominant vibration frequency in IL direction is twice that in CF direction [6]. The evaluation model of Eq. (8) did not reflect such frequency difference between the CF direction and the IL direction. Thus, we modified f_{1NF} in Eq. (8) to $2f_{1NF}$ for the IL direction. Fig. 4 shows that the predicted results are good. Table 3 gives the fitting and predicted values of the slop. The relative error in the total displacement direction is the smallest. This indicates that the proposed evaluation model is more reliable when it is employed to predict the conditioned maximum RMS of the total displacement for a long tensioned mooring tether undergoing VIV.

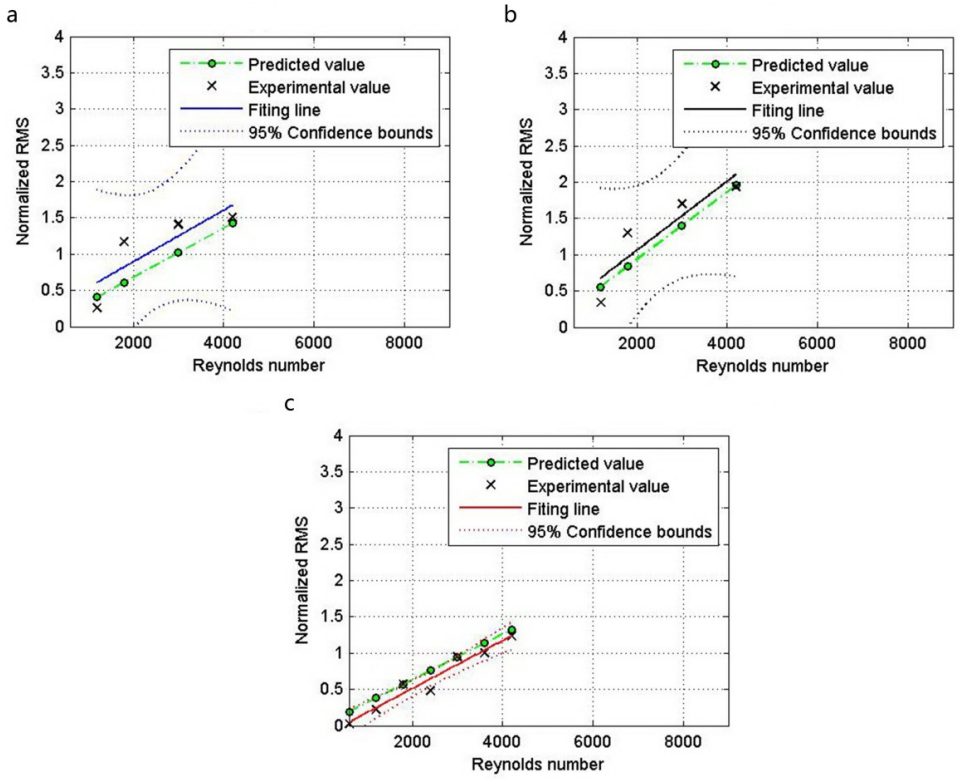

Fig. 4. Comparing predicted values with experimental values: (a) in CF direction; (b) in IL direction; (c) of total displacement.

Table 3. Fitting and Prediction values of the slop

Directions	Fitting ($\times 10^{-4}$)	Prediction ($\times 10^{-4}$)	Relative error (%)
CF	3.549	3.396	4.31
IL	3.306	3.152	4.66
TOTAL	4.761	4.658	2.16

4. Conclusions

An experiment was conducted in this paper to have an in-depth understanding on the variation of the maximum RMS of the displacement for a long tensioned tether undergoing VIV with the given flow velocity, and a model was established for the prediction of the maximum RMS of the displacement. Conclusions are as follows.

The maximum RMS of the displacement for a long tensioned mooring tether subjected to VIV linearly increases as the flow velocity increases if only the low order modes are excited at the corresponding flow velocities. This kind of maximum RMS of displacement is named conditioned maximum RMS of displacement in this paper. The magnitude of the conditioned maximum RMS of the displacement is evaluated by the proposed model. However, it is worth noticing that the model is more reliable when it is applied to the prediction of the conditioned maximum RMS of the total displacement.

Acknowledgements

This work was supported by the Construction Technology Program of Ministry of Transport (Grant No. 2013 318 740050).

References

[1] D. Ahrens, Submerged Floating Tunnels-A concept whose time has arrived, Tunn. Undergr. Sp. Tech. 12(2) (1997) 317-336.

[2] V. Jhingran, J.K. Vandiver, Incorporating the high harmonics in VIV fatigue predictions, in: Proceedings of the 26th International Conference on Offshore Mechanics and Arctic Engineering, OMAE2007-29352.

[3] H.N. Zheng, R.E. Price, Y. Modarres-Sadeghi, M.S. Triantafyllou, On fatigue damage of long flexible cylinders due to the higher harmonic force components and chaotic vortex-induced vibrations, Ocean Eng. 88 (2014) 318-329.

[4] M.L. Facchinetti, E. de Langre, F. Biolley, Vortex-induced travelling waves along a cable, Eur. J. Mech. B-Fluid. 23 (2004) 199-208.

[5] Z.B. Rao, J.K. Vandiver, V. Jhingran, Vortex induced vibration excitation competition between bare and buoyant segments of flexible cylinders, Ocean Eng. 94 (2015) 186-198.

[6] A.D. Trim, H. Braaten, H. Lie, M.A. Tognarelli, Experimental investigation of vortex-induced vibration of long marine risers, J. Fluid Struct. 21 (2005) 335-361.

[7] X. D. Wu, F. Ge, Y.S. Hong, Effect of traveling wave on vortex-induced vibrations of submerged floating tunnel tethers. Procedia Eng. 4 (2010) 153-160.

[8] X.D. Wu, F. Ge, Y.S. Hong, A review of recent studies on vortex-induced vibrations of long flexible cylinders, J. Fluid Struct. 28 (2012) 292-308.

[9] X.D. Wu, F. Ge, Y.S. Hong, An Experimental investigation of dual-resonant and non-resonant responses for vortex-induced vibration of a long slender cylinder, Sci. China Phys. Mech. 57(2) (2014) 321-329.

[10] T.L. Resvanis, V. Jhingran, J.K. Vandiver, S. Liapis, Reynolds number effects on the vortex-induced vibration of flexible marine risers, in: Proceedings of the ASME 2012 31st International Conference on Ocean, Offshore and Arctic Engineering, OMAE 2012-83565.

[11] H. Wu, D.P. Sun, L. Lu, B. Teng, G.Q. Tang, J.N. Song, Experimental investigation on the suppression of vortex-induced vibration of long flexible riser by multiple control rods, J. Fluid Struct. 30 (2012) 115-132.

[12] F. Ge, X. Long, L. Wang, Y.S. Hong, Flow-induced vibrations of long circular cylinders modeled by coupled nonlinear oscillators, Sci. China Phys. Mech. 52(7) (2009) 1086-1093.

[13] J.J. Gu, Y. Wang, Y. Zhang, M.L. Duan, C. Levi, Analytical solution of mean top tension of long flexible riser in modeling vortex-induced vibrations, Appl. Ocean Res. 41 (2013) 1-8.

[14] H. Lie, K.E. Kaasen, Modal analysis of measurements from a large-scale VIV model test of a riser in linearly sheared flow, J. Fluid Struct. 22 (2006) 557-575.

[15] L. Lee, D. Allen, Vibration frequency and lock-in bandwidth of tensioned flexible cylinders experiencing vortex shedding, J. Fluid Struct. 26 (2010) 602-610.